Computers & Graphics 99 (2021) 192–200

Contents lists available at ScienceDirect

Computers & Graphics

journal homepage: www.elsevier.com/locate/cag

Special Section on 3DOR 2021

SHREC 2021: 3D point cloud change detection for street scenes

Tao Ku[a,*], Sam Galanakis[a], Bas Boom[b], Remco C. Veltkamp[c], Darshan Bangera[d], Shankar Gangisetty[d], Nikolaos Stagakis[e], Gerasimos Arvanitis[e], Konstantinos Moustakas[e]

[a] Department of Information and Computing Sciences, Utrecht University, the Netherlands
[b] Imec One Planet Research Center, Wageningen, The Netherlands
[c] Department of Information and Computing Sciences, Utrecht University, The Netherlands
[d] KLE Technological University, Hubballi 580031, India
[e] Department of Electrical and Computer Engineering, University of Patras, Rio, Greece

ARTICLE INFO

Article history:
Received 1 April 2021
Revised 30 June 2021
Accepted 2 July 2021
Available online 10 July 2021

Keywords:
SHREC 2021
3D Point cloud change detection
Graph convolutional networks
Siamese networks

ABSTRACT

The rapid development of 3D acquisition devices enables us to collect billions of points in a few hours. However, the analysis of the output data is a challenging task, especially in the field of 3D point cloud change detection. In this Shape Retrieval Challenge (SHREC) track, we provide a street-scene dataset for 3D point cloud change detection. The dataset consists of 866 3D object pairs in year 2016 and 2020 from 78 large-scale street scene 3D point clouds. Our goal is to detect the changes from multi-temporal point clouds in a complex street environment.

We compare three methods on this benchmark, with one handcrafted (PoChaDeHH) and the other two learning-based (PointNet and SiamGCN). The results show that the handcrafted algorithm has balanced performance on all change while learning-based methods achieve overwhelming performance but suffer from the class imbalanced problem and may fail on minority classes. The randomized oversampling strategy applied in SiamGCN can alleviate this problem. Also, different siamese network architectures (PointNet and SiamGCN) contribute to the designing of a network for the 3D change detection task.

1. Introduction

Change detection (CD) has been one of the important topics in remote sensing, and has been applied in many practical areas such as forest monitoring, urban sprawl and earthquake assessment [1–3]. 3D change detection, as a subset of the general CD problem, is drawing more attention in the area of smart cities [4,5] with the advantages of free from illumination variations and perspective distortion due to the rich 3D geometric information. However, the high-cost acquisition equipment and limited data sources are the main barriers for the 3D CD applications [1,6]. Thanks to the rapid development of 3D acquisition devices, we are able to collect billions of points in a few hours. However, the analysis of the output data is still a challenging problem as there aren't generic, automated and accurate methodologies appropriate for all 3D change detection applications [7,8].

Change detection approaches can be generalized as direct comparison and classification-based comparison in [9]. Direct comparison is to detect changes directly from raw multi-temporal data. However, classification-based comparison is to classify objects, e.g. building, vegetation, and then detect their changes. Compared with direct comparison approaches, classification-based methods are easier to implement and reduce the difficulty of labelling changes in large-scale 3D point clouds.

Recent studies have focused on 3D data of the ground surface obtained from terrestrial laser scanners (TLS) and aerial laser scanners (ALS). Land cover and building related change detection [10–14] are the mainstream. High resolution 3D point clouds together with color images are combined as hybrid data sets to investigate both spatial and temporal changes. For unsupervised methods, most recent researches focus on calculating the historical differences directly. For example, digital elevation model (DEMs) difference based approaches [15,16] are proposed to identify locations and quantify spatial patterns of geomorphic changes. However, these approaches are usually based on the assumption that

* Corresponding author.
E-mail addresses: t.ku@uu.nl (T. Ku), samme.galanakis6@gmail.com (S. Galanakis), bas.boom@imec.nl (B. Boom), R.C.Veltkamp@uu.nl (R.C. Veltkamp), darshanbangera101@gmail.com (D. Bangera), shankar@kletech.ac.in (S. Gangisetty), nick.stag@ece.upatras.gr (N. Stagakis), arvanitis@ece.upatras.gr (G. Arvanitis), moustakas@ece.upatras.gr (K. Moustakas).

https://doi.org/10.1016/j.cag.2021.07.004

Table 1
Number of annotated objects in our Change3D benchmark.

Labels	nochange	removed	added	change	color_change	Total
Train set	421 (59.13%)	125 (17.56%)	68 (9.55%)	72 (10.11%)	26 (3.65%)	712
Test set	90 (58.44%)	25 (16.23%)	15 (9.74%)	17 (11.04%)	7 (4.55%)	154

the radiometric property of scanned objects are similar in different times which is actually not satisfied in real scenes. The direct and unsupervised difference calculation would introduce errors in change detection, especially for high resolution data. For supervised methods [17–19], there is usually a post-classification process to find valuable objects via an image analysis framework and then detect the changes using multi-modal and multi-temporal data. However, these approaches rely mainly on the imagery information. Furthermore, it is challenging to design a supervised model taking multi-modal and multi-temporal data as input.

In this SHREC track on 3D point cloud change detection for street scenes, we provide a cleaned and annotated 3D point cloud dataset obtained from mobile laser scanners (MLS). Objects in the dataset are initially roughly selected. Then, they are manually annotated with change labels. With the proposed dataset, we aim to compare and develop reliable and accurate change detection techniques for multi-temporal 3D street scenes.

We compare different methods on the proposed Street3D benchmark. The contributions are summarized as:

- We provide a unique classification-based 3D change detection dataset from a complex street environment. There are no other open 3D point cloud datasets released for our purpose.
- We evaluate different algorithms on the dataset and help finding solutions for 3D point cloud change detection tasks.
- The results show that the proposed siamese graph convolutional networks (SiamGCN) are good at extracting representative geometric features and can hereby outperform compar algorithms on the released Change3D dataset.

2. Change3D benchmark

In this comparative evaluation, we provide a change detection dataset named Change3D. The dataset is made publicly available at https://kutao207.github.io.

2.1. Dataset description

The dataset is provided by CycloMedia Technology and consists of annotated expert of interest in street level colored point clouds gathered in 2016 and 2020 in the city of Schiedam, the Netherlands using vehicle mounted LiDAR sensors. The dataset focuses on street furniture, with majority of labels corresponding to road-side although other objects such as advertisements, statues and garbage bins are included. Labeling was done through manual inspection. The 3D data from CycloMedia are generated from depth maps instead of original LiDAR scans, and they are already registered quite well [20].

We have selected over 78 annotated street-scene 3D point cloud pairs in the year of 2016 and 2020. Each point cloud pair represents a street scene in two different years and contains 866 object pairs of different change type in total. The statistics of the Change3D benchmark are summarized in Tab. 1. Each object pair is assigned one of the following labels:

(1) **nochange** (2) **removed** (3) **added** (4) **change** (5) **color_change**

- **nochange** refers to the case where there is no significant change between the two scans.
- **removed** refers to objects that exists in the first scan but are removed from the second scan.
- **added** refers to objects that do not exist in the first scan but are added during the second scan.
- **change** refers to the case where there is at least significant geometric change but also includes cases where there is also significant change in the RGB space. This includes being replaced by other objects. For example in Fig. 1 a small blue sign is added whilst the rest of the sign stays the same.
- **color_change** refers to the case where there is not significant geometric case but significant change in the RGB space. For example, in Fig. 1 (b), content of an advertisement changed but the rest of the cloud is the same.

2.2. Labeling format

Each data point consists of the coordinates of a point of interest and the corresponding label. These have been placed on or at the base of the objects. A first step for preparing the points for input to a model may be picking all points within a certain x-y radius of the points of interest (resulting cylinders as seen in Fig. 1) from both point clouds. In most cases, apart from the ground this will give a fairly clear representation of the object. There are though cases where this will include other objects (for example signs that are close together) or parts of trees that are above the object.

Corresponding point clouds are saved with file names starting with the same integer (the scene number). The classifications are stored in csv files which also start with the same scene number. The coordinates contained in the csv file correspond to the points of interest.

2.3. Task and evaluation

Our task is to classify the changes of meaningful objects from two different years' 3D point clouds in a complex street environment. We provide scene-level 3D point clouds of year 2016 and 2020 and the corresponding center of meaningful objects. Participants are encouraged to try out different methods for our task.

We adopt the Overall Accuracy (OA) and mean Intersection over Union (mIoU) metrics in our 3D change detection task.

Generally, OA reports the percent of points in the data set which are correctly classified:

$$\mathrm{OA} = \frac{\mathrm{N_{correct}}}{\mathrm{N_{total}}} \tag{1}$$

where $\mathrm{N_{correct}}$ is the number of correctly classified points and $\mathrm{N_{total}}$ is the total number of points. mIoU is the average of per-class IoU. The IoU of class i is defined as:

$$\mathrm{IoU}_i = \frac{\mathrm{TP}_i}{\mathrm{GT}_i + \mathrm{Pred}_i - \mathrm{TP}_i} \tag{2}$$

where TP_i, GT_i, Pred_i denote the correctly classified number of points, the ground truth point number, and the predicted point number for class i, respectively. The classes are *nochange*, *removed*, *added*, *change* and *color_change*.

3. Methods

3.1. PoChaDeHH: Point cloud change detection with hierarchical histograms

This method is contributed by authors [Nikolaos Stagakis, Gerasimos Arvanitis and Konstantinos Moustakas]. In the follow-

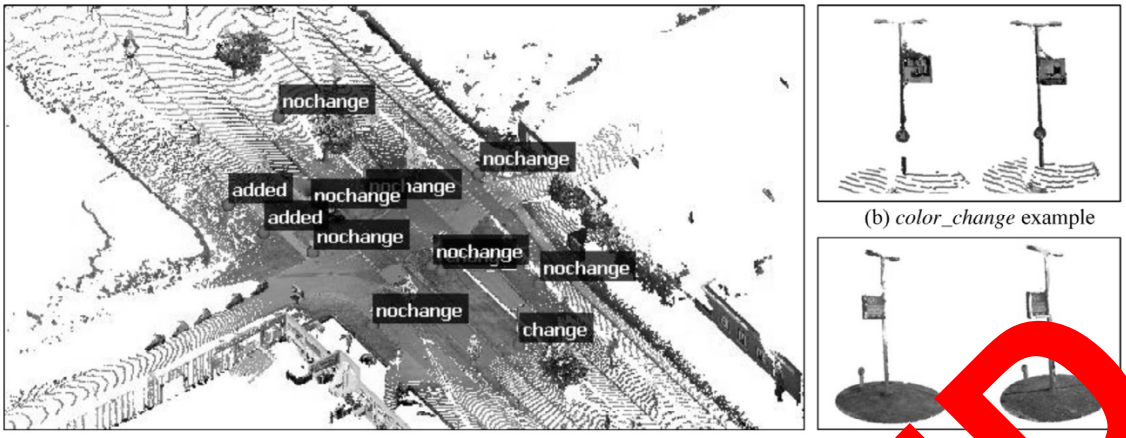

(a) Single street scene with multiple changed objects.

(b) *color_change* example

(c) *c* and *a* example

Fig. 1. An example of our Change3D dataset.

ing paragraphs, we will briefly describe all the steps that we follow for the change detection approach, named Point Cloud Change Detection with Hierarchical Histograms (PoChaDeHH) that we developed. The source code of our work is freely available at https://github.com/Stagakis/shrec21_changedetection.

3.1.1. Notation and basic definitions

- as "point-of-interest" we refer to the given point that specifies the area (subscene) in which the object-of-interest exists. The points are found in the csv file of the respective scene.
- as "subscene" we refer to the segment of the original point cloud scene in which the object-of-interest lies. The subce extracted by centering a cylinder on the point of interes particular, we use a modified version of the python script p vided for visualizing the subscenes to save the ene in separate ".las" file.
- as "object-of-interest" we refer to the spec object the subscene that we need to check about possi han defined based on the given point-of-i est. st of the objects extracted by the cylinder (if) are cons d and handled as outliers and noise.

3.1.2. Pre-processing of the sce

The subscenes of the g dataset usual nsist of outliers, incomplete and/or noisy jects w ile other u lated objects are spatially close to our ect-of erest. To simplify the subscene, we remove these objec plying a ries of processing steps. These steps des d belo e repe d for each subscene of all scenes for bo hrono eas.

3.1.3. Pla rea re

Firstly, w to r the floor of the extracted subscene. To do that, we ect the plane with the most inliers of each subscene and disca em. This step helps us later to separate the different objects th may appear in the subscene. In Fig. 2, we present an example of two subscenes and in Fig, 3 the results after the floor removal.

Note here that after this step it is possible that all the information of the subscene to have been removed (i.e., it there was only a flat area). In that case, we either save the original subscene, for later deciding whether the subscene is colorchanged or not, or we replace the subscene with a dummy point at [0 0 0]. The latter is done in the case of geometric classification.

3.1.4. Clustering

We estimate density clusters of each subscene in order to reject these objects that are far away from the object-of-interest and they

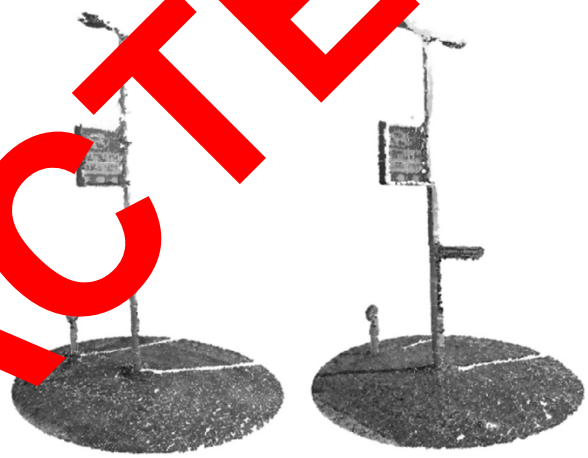

Fig. 2. Example of original subscenes for the dataset of 2016 and 2020, correspondingly.

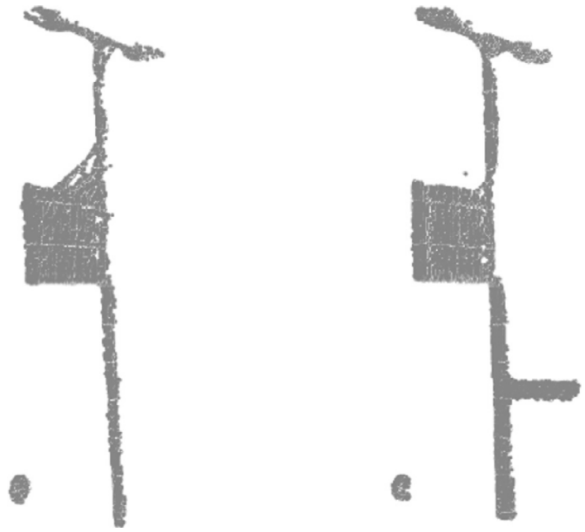

Fig. 3. Original subscenes without the large plane area.

are not semantically related with it. In this step, we use an adaptive approach of the DBSCAN [21] algorithm that separates the objects of the subscene into clusters based on their density. To mention here that we select and merge these cluster(s) which are close

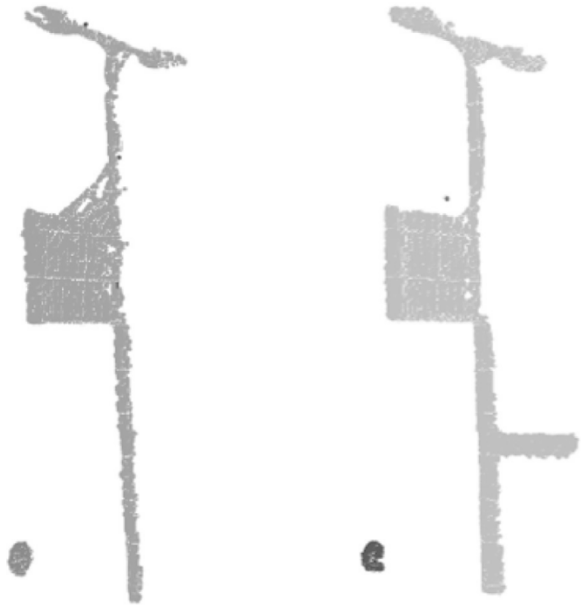

Fig. 4. Results after the process of clustering.

Fig. 5. Heatmap of the m distance between each point of the one object-of-interest closest points e other.

to the point-of-interest (i.e., regarding a predefined threshold). In Fig. 4, we present an example where more than one objects are presented in the subscene. However, only one of them is related with the real object-of-interest that we want to compare, so we have to remove all the other unrelated objects.

3.1.5. Registration

Once, we have found the corresponding clusters, which are lated to the given point-of-interest, we apply a registration proce to the cluster(s) of the newest date with the co g clus ter(s) of the oldest date.

3.1.6. Comparison between registered point cloud

To decide the class of each situati we fi estimate the mean euclidean distance of each poi f the one cl with the 15 closest point of the other clus ing in this w a list of pairs and their corresponding distance. A mple that visualizes the heatmap of this distanc presented i 5. Then, we create two histograms, usin ese distances, wit n equal number of bins (i.e., 50) in or to be ly compared since the values are not normalized, as n Fig. 6. These histograms represent each one for the cor ding tw lusters of each subscene. According to t togra into account only the high values of d nces uming ey lie in the histograms between 4 bins.

Additio mall differences between the two compared ob f-interest (i.e., change case) we search for vertices that do no ear in the list of pairs. The number of these unrelated vertices be used to show a possible change between the two objects.

3.1.7. Color comparison between clustered point clouds

After the initial comparison for determining the geometric class of the object-of-interest, we take another step to find color changes between the point clouds and refine our classification. Given the nature of the colorchanged class we can assume that, regarding the geometry, color changed point clouds are a subset of the nochange class. Thus, we implement a histogram comparison between point clouds that receives as input only the nochange classified objects in the previous step and classifies them as either nochange or colorchange. The color comparison is done in the HSV space to reduce th effect of lu osity changes and the histograms are aligned. Lo g at the s stical distribution of the histogram distance for eac ss, we se a threshold to decide whether the input object is e nochange class or should be classified as colorhanged.

entire pipeline of our work is shown in Fig. 7.

3.2. HGI-CD: 3D point cloud change detection for street scenes

This method is contributed by authors [Darshan Bangera and Shankar Gangisetty]. In this work, we propose a hybrid learning-based 3D change detection of bi-temporal point clouds as shown in Fig. 8. Initially, we calculate the change between 2016 and 2020 point clouds by applying a point-to-point Hausdorff distance [22]. Hausdorff distance is the greatest of all the distances from a point in one set to the closest point in the other set. We then designed a Siamese classification network [23] to detect the changes between point cloud street scenes.

3.2.1. Data pre-processing

Given the 3D point cloud scenes of 2016 and 2020 as inputs to the proposed hybrid learning-based framework as shown in Fig. 8. Initially the 3D objects present in 2016 and 2020 scenes are extracted by considering the points that lie within a cylindrical region around the point of interest. Let $(n \times 3)$ and $(m \times 3)$ represent the extracted 2016 and 2020 3D objects, where n and m are the number of points in 2016 and 2020 with (x, y, z) as point coordinates.

We then isolate the 3D objects of 2016 $(n' \times 3)$ and 2020 $(m' \times 3)$ from the ground surface by eliminating the large planes that are parallel to the ground surface and pass through the point of interest as shown in Fig 8. Any of the outliers present are removed using statistical outlier removal technique. If there are no points within the extracted region, we add the point of interest as the sole point in the 3D object.

3.2.2. Change computing

To calculate the geometrical changes between the 2016 and 2020 point clouds, we perform a Hausdorff distance computing between each point in the 2016 object to its nearest neighbour in the

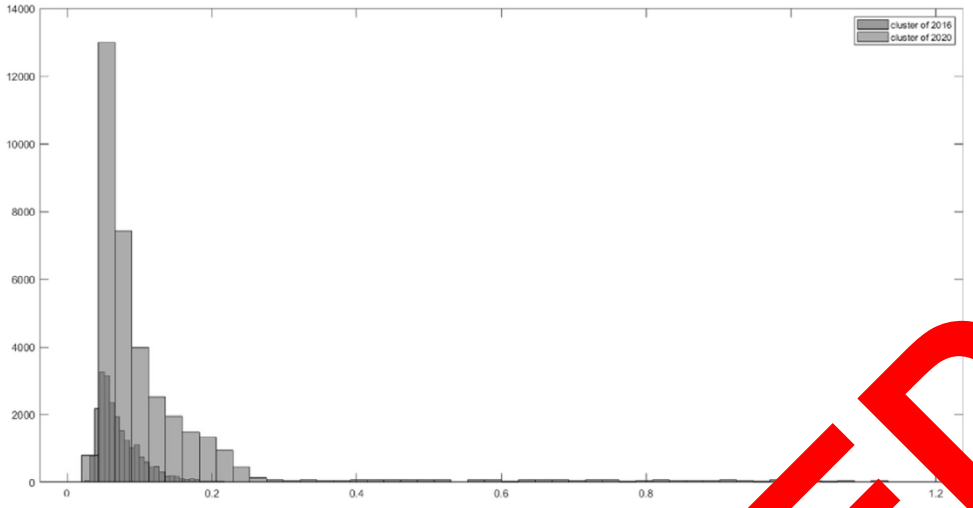

Fig. 6. Histograms of the mean distance between each point of a cluster and the close[illegible] other.

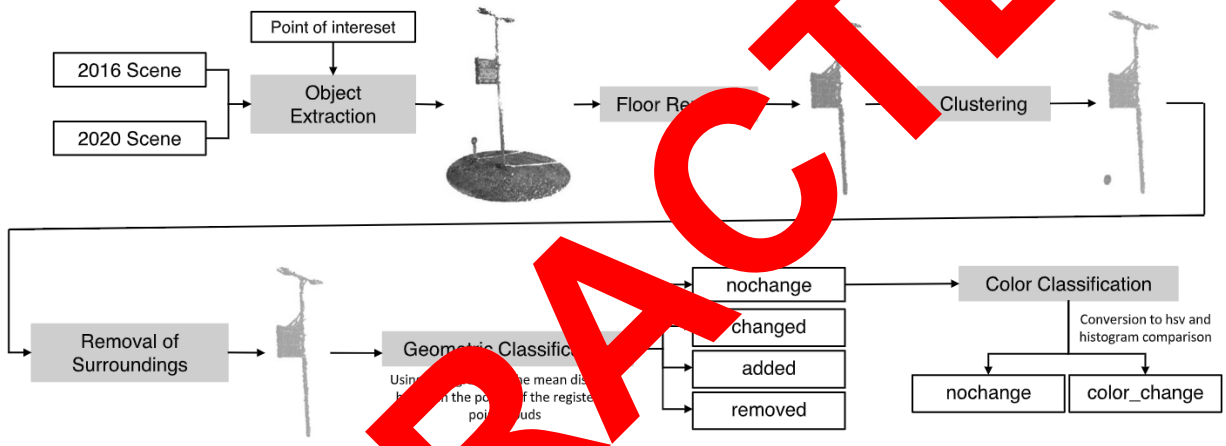

Fig. 7. Histogram[illegible]ne me[illegible]ance between each point of a cluster and the closest points of the other.

2020 point cloud and vice-versa[illegible] th[illegible]erform thresholding to select the points with significant change in[illegible]ition.

After the change comp[illegible]ion, we build[illegible]r change graphs and geometric change g[illegible]hs. In the color cha[illegible]ge graphs, calculation of the changes[illegible] colour[illegible]ace is performed by first averaging the RGB values i[illegible]ctive re[illegible] green and blue bins. A colour space poi[illegible]loud i[illegible]nerated[illegible] taking the averaged RGB values. The c[illegible]olor sp[illegible]iculated by applying a point-to-point H[illegible]dorff d[illegible]ance. Fo[illegible]ch RGB point with significant change, [illegible]orresp[illegible](x, y, z) coordinate from the point cloud is taken. Th[illegible]est nei[illegible]ours (KNN) algorithm is used to generate a graph[illegible] color and geometrical change point clouds of 2016 and 2020 3[illegible]jects, respectively. The fast point feature histograms (FPFH) [24][illegible]e calculated for each point as their node features. The results from the three streams (i.e., color change, 2016 points geometry, 2020 points geometry) are then concatenated and passed to multi layer perceptrons to generate the output. In the LiDAR scene scenarios where there are no points of significant change in both 2016 and 2020 point clouds, the object is directly labelled as *nochange*.

3.2.3. Training

We train the hybrid learning-based model using the graph node features and the edge indices as shown in Fig. 9. The loaded data is of dimensions (N, G) for geometrical change detection and (N, C) for colour change detection, where N is the number of nodes of the 3D object, G is the total features selected for FPFH along the RGB values of the node and the RGB values of its nearest neighbour. The color change graphs and geometric change graphs data is fed to a Siamese graph convolutional networks (GCNs) [25] followed by inception networks [26]. Each of the GCN accepts the node features and edge indices as its input as shown in Fig. 9. The GCN network performs convolutions on the node features but maintains the structure of the graph. The obtained intermediate results have 80 dimensions which is fed to an Inception V1 network as specified in [26]. Each parallel stream (i.e., the color and geometric change) learn to detect if a set of points represent a changed part or not. Global mean pooling is performed on the 180 dimensions output of each stream to ensure that classification is done on the graph as a whole. The outputs are concatenated and fed to a multi-layered perceptron to provide the final labels. The point cloud change detection class labels are *added*, *removed*, *nochange*, *change*, and *color_change*.

3.2.4. Implementation details

We train the model using the Adam optimizer with a learning rate of 0:001 and a decay rate of 0:001. Empirical we set a threshold of 0:2 to select the points of significant geometric change and generate a k-NN graph with $k = 10$. Since the data are imbalanced,

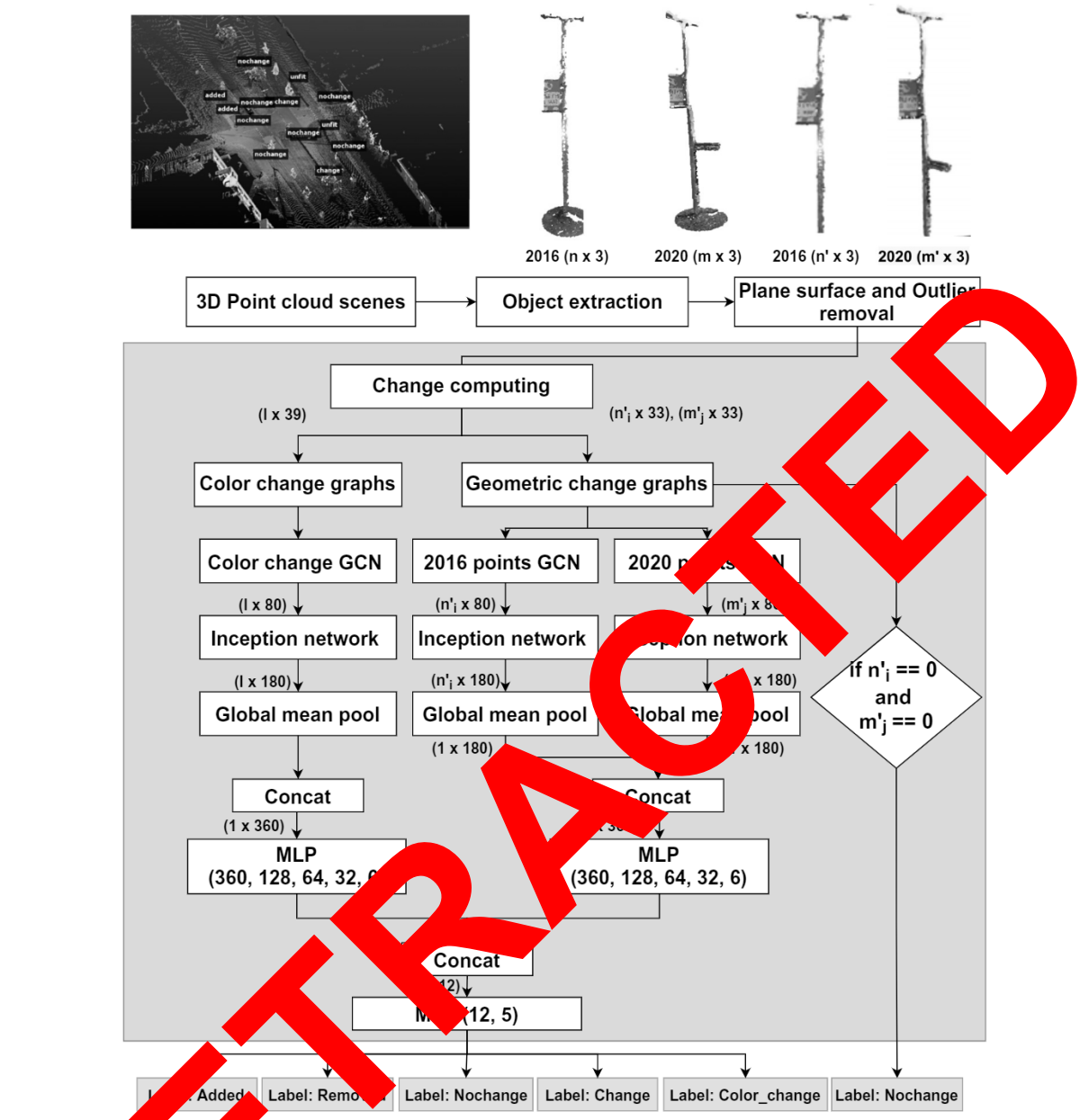

Fig. 8. Proposed hybrid learning-based point cloud change detection.

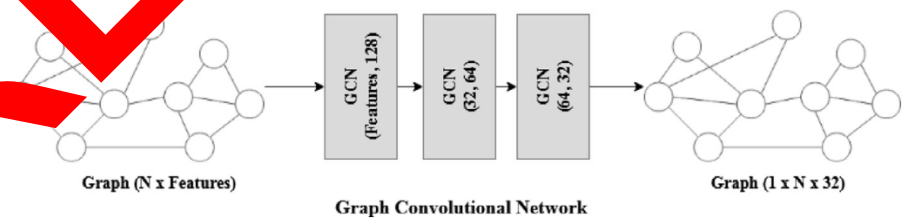

Fig. 9. Graph convolution network for point cloud change detection.

we perform data augmentation on each of the different classes by considering jitter and rotation to balance the dataset. We used a train : validation split of 80 : 20 for experimental analysis. The model is trained on hardware comprising of 16 GB CPU and a single NVIDIA Quadro P600 GPU.

After acceptance the clean code will be released. For evaluation the code at following GitHub link is submitted: https://github.com/darshanbangera/3D-Change-Detection.

3.3. SiamGCN: Siamese graph convolutional network for 3D point cloud change detection

This method is contributed by authors [Tao Ku, Sam Galanakis, Bas Boom and Remco C. Veltkamp]. In this section, we introduce a Siamese Graph Convolutional Network (SiamGCN) for 3D point cloud change detection. The edge convolution operator is adopted to extract representative features from point clouds. Then,

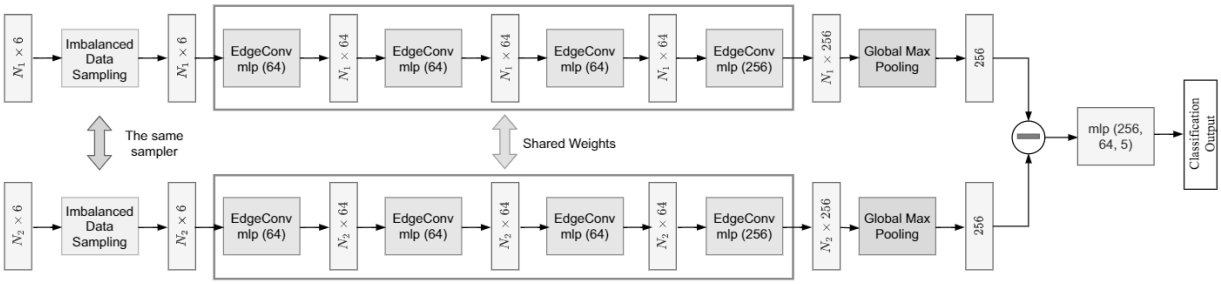

Fig. 10. The network architecture of the proposed SiamGCN.

a siamese architecture [27] based on the graph convolutional networks is proposed to identify the change type of any two input point sets from two different years. The code of our approach is publicly available at https://github.com/kutao207/SiamGCN.

3.3.1. Preprocessing

We design a siamese network for the task. However, the provided data are in the form of large point clouds and only object center coordinates are given. The size and shape of the objects are uncertain. To correctly identify the change type, we need to properly extract object pairs around given center coordinates and input these point cloud pairs to our proposed network for training and evaluation. Since the task is to classify change types instead of object classes, we don't need to extract the objects correctly. Considering that the point clouds are well registered, we extract the cylinders around the given centers with an experimental distance of 3 m for all samples. We don't expect the extracted point c have the same input point number as our network is well-desi to deal with this issue.

3.3.2. Network architecture

As shown in Fig. 10, the proposed Sia cons of two branches of graph convolutional netwo share the same weights. The point clou rom tw ferent times are fed into corresponding branch a utput two dimension vectors through the global max p g er. By subtr g these two vectors, we use an MLP to ge the fi lassification output.

Imbalanced Data Sampl As shown in . 1, the data are class-imbalanced. Around % samples are la ed as nochange and only around 3% a abelled color_change, which will lead to a biased training pr result in failure cases in predicting minority classes. In o to add this problem, we adopt the randomize ampli net in [28]. The general idea is to randoml plica samples e minority class to make sure that sam of eac lass has the same probability being adopted in the trai p

Graph Co ction: In order to apply graph convolution on point clouds, we d to construct graphs for input points. Considering the irregular a format of point clouds, we use graphs to encoding the geometric relations among points. For a point cloud with N points, suppose $X \in \mathcal{R}^{N\times 3}$ denotes the XYZ coordinates of N points. A graph $\mathcal{G} = (\mathcal{V}, \mathcal{E})$ represents the local structure, where $\mathcal{V} = 1, 2, \cdots, n$ and $\mathcal{E} \subseteq \mathcal{V} \times \mathcal{V}$ are vertices and edges. In our approach, we use the k-nearest neighbor (kNN) algorithm to build the graph of X and obtain corresponding adjacency matrix $\mathbf{A}$. We set the kNN query number as 16 throughout our experiments.

Graph Convolution: Inspired by [27], we adopt the edge-conditioned graph convolution operator in our proposed SiamGCN architecture. Edge convolution [27] is adopted to dynamically update the edge features. Generally, the edge convolution is to apply a channel-wise symmetric aggregation operation on the edge features. Mathematically,

$$\mathbf{x}_i^{(k)} = \mathrm{ReLU}(\theta_m \cdot (\mathbf{x}_j^{(k-1)} - \mathbf{x}_i^{(k-1)}) + \phi_m \cdot \mathbf{x}_i^{(k-1)}) \tag{3}$$

where θ_m and ϕ_m are the eights of fil can be implemented as a shared ML denot he Euc n inner product. $\mathbf{x}_i^k$ denotes the i-th edge ure tput of he k-th layer output.

Then, we adopt grap volutio cept in [29] to encode geometric infor on as

$$\mathbf{Y} = \mathbf{AXW} \tag{4}$$

where $\mathbf{X} = \{\mathbf{x}_1, \cdots, \mathbf{x}_N\} \in \mathbb{R}^{N\times C}$ is the input features, $\mathbf{Y} \in \mathbb{R}^{N\times D}$ is the output, $W \in$ denotes the weight matrix, and $\mathbf{A}$ is th djacency matrix.

4. ults and ussion

4.1. Exp t results

itative evaluation results on the Change3D benchmark are ummarized in Tab. 2. Overall Accuracy (OA) and mean Intersection over Union (mIoU) are evaluated for all classes. We have also calculated the classification accuracy and IoU for each class respectively. In Fig. 11, confusion matrices are plotted to intuitively show the strength and weakness of each method.

We have evaluated the three submitted methods: PoChaDeHH, HGI-CD and SiamGCN. PoChaDeHH is based on hand-crafted detectors, while HGI-CD and SiamGCN are learning-based and both adopt graph convolution networks and Siamese network architecture.

From Tab. 2, it is straightforward that SiamGCN outperforms the other two methods on accuracy and IoU. PoChaDeHH, as a non-learning based method can achieve 61.04% overall accuracy and relatively balanced performance on classes. HGI-CD, as one of the learning-based methods, achieves good result on classifying majority class *nochange*, but fails on minority classes *change* and *color_change*. The SiamGCN has very good performance on the dataset, especially on minority classes which achieves 95.24% and 98.57% accuracy on minority classes *change* and *color_change*.

4.2. Discussion

Handcrafted *v.s.* **Learning-based**: Three algorithms including one handcrafted and two learning-based are evaluated on the 3D change detection dataset. Although the handcrafted algorithm can achieve relatively balanced results on the overall and per-class accuracy and mIoU, it's still obvious that learning-based methods can achieve overwhelming performance.

Class imbalance: Class imbalance poses a challenge for learning-based modeling as most machine learning algorithms are designed with the assumption of an equal number of examples for each class. However, due to the limitations of data acquisition, class-imbalanced problem cannot be avoided. Around 60% objects

Table 2
Quantitative results on the Change3D benchmark.

Method	OA (%)	mIoU (%)	nochange		removed		added		change		color_change	
			Acc.	IoU	Acc.	IoU	Acc.	IoU	Acc.	IoU	Acc.	IoU
PoChaDeHH	61.04	30.22	76.70	**61.06**	48.00	31.58	66.70	40.00	5.90	4.17	28.60	14.29
HGI-CD	53.90	17.17	81.11	55.30	28.00	16.28	20.00	14.29	0.00	0.00	0.00	0.00
SiamGCN	**92.42**	**76.63**	**84.25**	55.03	**89.80**	**72.07**	**94.70**	**89.82**	**95.24**	**69.57**	**98.57**	**96.67**

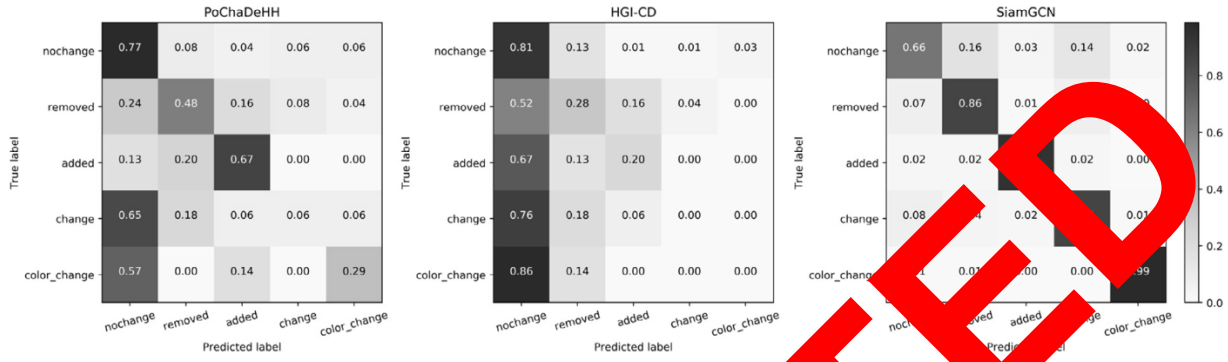

Fig. 11. Confusion matrix for all the three comparison algorithms. The x-axis represents the predicted la… the y-axis den… groundtruth labels. In this figure, each subfigure shows clearly the classification ability of each algorithm. We normalized each row of t… confusi… atrix so that it is intuitive to show the probability of correct predictions and incorrect predictions.

Table 3
The comparison between concatenation operator and subtraction operator in SiamGCN.

	OA (%)	nochange	removed	added	change	color_change
Concat	76.54	39.60	76.06	88.37	82.64	97.97
Sub	92.42	84.25	89.80	94.70	95.24	98.57

are labelled as *nochange* and only 3.65% labelled … *change*. Hence, it is important to deal with the class im… nce f… he participated algorithms. SiamGCN adopts ran… zed o… ampling metric to avoid the class-imbalanced pr… lem … results on minority classes. However, … CD lac… s procedure and fails on the minority classes w… indicates t… portance of resampling part when desig… a… gorithm fo… e class-imbalanced change detection dataset.

Network architecture: … en adopting … p learning based methods, the network d… gn is extremely im… rtant for robust and effective modelin… or thi… change detection task, both HGI-CD and SiamGCN … t… e graph convolutional networks and Siamese architectur… there … still many differences. When dealin… e out… fea… es of the siamese network, HGI-CD us… conc… enation … ator while SiamGCN adopts a subtracti… operato… which makes a difference to the final performance. In … the importance of these two operators, we co… the performance of these two operators in the SiamGCN metho… e results are summarized in Tab. 3. The subtraction operator g… ly increases the performance on both overall and per class accuracy. Although the concatenation operator has been widely used in classification and semantic segmentation, subtraction is more natural and reasonable for change detection as it is to classify the differences.

5. Conclusions

In conclusion, this comparative evaluation contributes to 3D point cloud change detection for street scenes with multiple approaches. We provide a street-scene 3D change detection dataset composed of 78 scans with 866 annotated object pairs in year 2016 and 2020. Five class labels are included for the change type. W… ntroduce three novel and different methodologies including o… handcrafte… ethod and two learning-based methods (HGI-CD… d SiamGC… It shows that learning-based can achieve overwhe… per… ance on the dataset. SiamGCN solves the class-imbalanc… problem by adopting randomized oversampling and … oses a well-designed siamese graph convolutional network ar… for the 3D change detection task. Comparison results … hows that over-sampling and using subtraction operator are the key for the SiamGCN to achieve the best performance on the released Change3D benchmark. The three compared algorithms contribute on how to design a proper framework for the 3D change detection task.

Declaration of Competing Interest

The authors declare that they have no known competing financial interests or personal relationships that could have appeared to influence the work reported in this paper.

No funding was received for this work.

We confirm that we have given due consideration to the protection of intellectual property associated with this work and that there are no impediments to publication, including the timing of publication, with respect to intellectual property. In so doing we confirm that we have followed the regulations of our institutions concerning intellectual property.

CRediT authorship contribution statement

Tao Ku: Methodology, Software, Writing – original draft. **Sam Galanakis:** Data curation, Writing – review & editing. **Bas Boom:** Data curation. **Remco C. Veltkamp:** Writing – review & editing. **Darshan Bangera:** Methodology, Software, Writing – original draft, Writing – review & editing. **Shankar Gangisetty:** Methodology, Software, Writing – original draft, Writing – review & editing. **Nikolaos Stagakis:** Methodology, Software, Writing – original draft, Writing – review & editing. **Gerasimos Arvanitis:** Methodology, Software, Writing – original draft, Writing – review & editing. **Konstantinos Moustakas:** Methodology, Software, Writing – original draft, Writing – review & editing.

References

[1] Qin R, Tian J, Reinartz P. 3D change detection – approaches and applications. ISPRS J Photogramm Remote Sens 2016;122:41–56.

[2] Tewkesbury AP, Comber AJ, Tate NJ, Lamb A, Fisher PF. A critical synthesis of remotely sensed optical image change detection techniques. Remote Sens Environ 2015;160:1–14.

[3] Song D-X, Huang C, Sexton JO, Channan S, Feng M, Townshend JR. Use of landsat and corona data for mapping forest cover change from the mid-1960s to 2000s: case studies from the eastern united states and central brazil. ISPRS J Photogramm Remote Sens 2015;103:81–92. Global Land Cover Mapping and Monitoring

[4] Daniel S, Doran M-A. Geosmartcity: Geomatics contribution to the smart city. In: Proceedings of the 14th Annual International Conference on Digital Government Research. New York, NY, USA: Association for Computing Machinery; 2013. p. 65–71. ISBN 9781450320573.

[5] Zolanvari SMI, Ruano S, Rana A, Cummins A, da Silva RE, Rahbar M, et al. Dublincity: Annotated lidar point cloud and its applications. In: 30th British Machine Vision Conference 2019, BMVC 2019, Cardiff, UK, September 9–12, 2019. BMVA Press; 2019. p. 44.

[6] Xiao W, Vallet B, Paparoditis N. Change detection in 3d point clouds acquired by a mobile mapping system. ISPRS Annals of Photogrammetry, Remote Sensing and Spatial Information Sciences 2013;1(2):331–6.

[7] Karantzalos K. Recent advances on 2d and 3d change detection in urban environments from remote sensing data. Computational Approaches for Urban Environments 2015:237–72.

[8] Mazzanti P, Caporossi P, Brunetti A, Mohammadi FI, Bozzano F. Short-term geomorphological evolution of the poggio baldi landslide upper scarp via 3d change detection. Landslides 2021:1–15.

[9] Singh A. Review article digital change detection techniques using remotely-sensed data. Int J Remote Sens 1989;10(6):989–1003.

[10] Boehm HV, Liesenberg V, Limin SH. Multi-temporal airborne lidar-survey and field measurements of tropical peat swamp forest to monitor changes. IEEE J Sel Top Appl Earth Obs Remote Sens 2013;6(3):1524–30.

[11] Ventura G, Vilardo G, Terranova C, Sessa EB. Tracking and evolution of complex active landslides by multi-temporal airborne lidar data: the montaguto landslide (southern italy). Remote Sens Environ 2011;115(12):3237–48.

[12] Jaboyedoff M, Oppikofer T, Abellán A, Derron M-H, Loye A, Metzger R, et al. Use of lidar in landslide investigations: a review. Natural hazards 2012;61(1):5–28.

[13] Abellán A, Vilaplana JM, Calvet J, García-Sellés D, Asensio E. Rockfall itoring by terrestrial laser scanning–case study of the basaltic rock at castellfollit de la roca (catalonia, spain). Nat Hazards Earth Syst 2011;11(3):829–41.

[14] Mineo S, Pappalardo G, Mangiameli M, Campolo S, Mussum kfall ana ysis for preliminary hazard assessment of the cliff of en castle (sicily). Sustainability 2018;10(2):417.

[15] James LA, Hodgson ME, Ghoshal S, Latiolais MM. Geomorphic change detection using historic maps and dem differencing: the temporal dimension of geospatial analysis. Geomorphology 2012;137(1):181–98.

[16] Rumsby B, Brasington J, Langham J, McLelland S, Middleton R, Rollinson G. Monitoring and modelling particle and reach-scale morphological change in gravel-bed rivers: applications and challenges. Geomorphology 2008;93(1–2):40–54.

[17] Tzotsos A, Karantzalos K, Argialas D, Weng Q. Multiscale segmentation and classification of remote sensing imagery with advanced edge and scale-space features. In: Scale Issues in Remote Sensing. Wiley Online Library; 2014. p. 170–96.

[18] Berger C, Voltersen M, Eckardt R, Eberle J, Heyer T, Salepci N, et al. Multi–modal and multi-temporal data fusion: outcome of the 2012 grss data fusion contest. IEEE J Sel Top Appl Earth Obs Remote Sens 2013;6(3):1324–40.

[19] Schneider A. Monitoring land cover change in urban and peri-urban areas using dense time stacks of landsat satellite dat data mining approach. Remote Sens Environ 2012;124:689–704.

[20] Someren Bv. Neural multi-view segment -aggregati joint lidar and image object detection; 2017.

[21] Ester M, Kriegel H-P, Sander J, Xu X. A y-based algo for discovering clusters a density-based algo m for d ring clust in large spatial databases with noise. In: Proc gs of the Inte onal Conference on Knowledge Discovery an a Mining. AAAI . p. 226–31.

[22] Huttenlocher DP, Klander GA, Ru ge W. C ng images using the hausdorff distance. IEEE Patte ial Mach Intell 1993;15(9):850–63.

[23] Melekhov I, Kannala Rah se netwo atures for image matching. In: 23rd Internati Confer n Patter ognition, ICPR 2016, Cancún, Mexico, Decem 4–8, 2016. IE 16. 8–83.

[24] Rusu RB, Bl Beetz M. Fast ture histograms (FPFH) for 3d registration. I 00 International ference on Robotics and Automation, ICRA 2009 Kobe, Ja May 12–17, 2009. IEEE; 2009. p. 3212–17.

[25] Wu F, AHS Jr, Zhang C, Yu T, Weinberger KQ. Simplifying graph con- networks. In: huri K, Salakhutdinov R, editors. Proceedings of 36th International Conf ce on Machine Learning, ICML 2019, 9–15 June 019, Long Beach, California, USA. Proceedings of Machine Learning Research, 7. PMLR; 201 6861–71.

[2 egedy C, Liu ia Y, Sermanet P, Reed SE, Anguelov D, et al. Going deeper h convoluti n: IEEE Conference on Computer Vision and Pattern Recog- CVPR , Boston, MA, USA, June 7–12, 2015. IEEE Computer Society; 20

[27] Wang Y, Sun Y, Liu Z, Sarma SE, Bronstein MM, Solomon JM. Dynamic graph NN for learning on point clouds. ACM Trans Graph 2019;38(5):146:1–146:12.

GEAPA, Prati RC, Monard MC. A study of the behavior of several methods for balancing machine learning training data. SIGKDD Explor 2004;6(1):20–9.

[29] Chen S, Varma R, Sandryhaila A, Kovacevic J. Discrete signal processing on graphs: sampling theory. IEEE Trans Signal Process 2015;63(24):6510–23.